Influence of Ceramic Supports on Microwave Heating for Composite Dielectric Food Slabs

Tanmay Basak and A. Meenakshi
Dept. of Chemical Engineering, Indian Institute of Technology, Madras, Chennai 600 036, India

DOI 10.1002/aic.10804
Published online March 14, 2006 in Wiley InterScience (www.interscience.wiley.com).

A detailed theoretical analysis has been carried out to study efficient heating of one-dimensional (1-D) composite dielectric food slabs due to microwaves. Current study involves processing of beef with oil layers with/without ceramic support for various cases, such as the support and/or oil layer is directly exposed to microwaves (case 1), the beef layer is directly exposed to microwaves (case 2) and oil-beef layers and the ceramic supports are exposed to microwaves at both the sides (case 3). A preliminary analysis on microwave heating has been carried out for beef-oil composite without any support and the maxima in average power corresponding to resonances occur at various sample thicknesses for all cases. The detailed spatial distribution for various cases illustrates that for small oil thicknesses, heating rate is less and greater heating rate would correspond to larger oil thicknesses specially for case 1. The similar analysis has been extended for all cases with oil layer directly attached with ceramic supports (Al_2O_3 and SiC). The detailed analysis on spatial distribution of temperature and power during one side incidence illustrate that the greater thermal runaway occurs for case 2 with Al_2O_3 support corresponding to smaller oil thickness whereas SiC support may cause thermal runaway for larger oil thicknesses. For distributed microwave incidences (case 3), it is observed that Al_2O_3 support may cause thermal runaway whereas SiC support may reduce the thermal runaway, based on suitable distribution of microwaves at both sides. © 2006 American Institute of Chemical Engineers *AIChE J,* 52: 1995–2007, 2006

Introduction

Electromagnetic radiations in the frequency range 300 MHz to 300 GHz are known as microwaves, and the typical wave lengths of microwaves are within few mm to 30 cm. The longer microwaves, those closer to a foot in length, are the waves which heat food in a microwave oven whereas shorter microwaves are used for radar in the weather forecasts. Unique advantages of microwave processing are heating, drying, chemical reactions, thawing-tempering and many more (Ayappa et al., 1991, 1992; Basak and Ayappa, 1997, 2001; Chamchong and Datta, 1999a, 1999b; Massoudi et al., 1979; Ohlsson and Risman, 1978; Rattanadecho, 2004; Shin et al., 2001; Weil, 1975; Xu et al., 2004). Microwaves propagate through the material, and the accompanying transport processes result in dissipation of electric energy into heat, which lead to the term "volumetric heat generation." In contrast, during conventional heating the heat is radiated from the burner to the surface of the material and the material is heated due to surface heat flux. During microwave heating, the material dielectric loss which is a function of frequency of microwaves, is responsible to convert electric energy into heat. Dielectric response of various materials plays an important role to carry out efficient material processing, and a significant amount of earlier research was devoted to understand the physics of microwave assisted transport and heating characteristics.

The detailed analysis on modeling of microwave heating has been carried out by Ayappa et al. (1991, 1992), and their investigations were based on heating of 1D slabs and 2D cylinders. They have carried out detailed theoretical analysis

Correspondence concerning this article should be addressed to T. Basak at tanmay@iitm.ac.in

on microwave propagation and heat transport for various multiphase and multilayered samples. The localized or nonuniform heating in samples is found to occur due to volumetric heating effects, and considerable further studies were devoted on analysis of maxima in power or "resonances" due to microwave propagation. A few earlier research (Ayappa et al., 1997; Ayappa, 1999) was carried out to investigate maxima in average power or heating rate which corresponds to a fixed sample dimension in 1-D slabs and 2-D cylinders, and the suitable relationships between occurrence of resonance with sample size were established. Microwave heating and transport models were further applied for thawing and heating of multiphase systems in recent investigations (Basak and Ayappa, 1997, 2001, 2002; Basak, 2003, 2004a, 2004b; Lee and Marchant, 2004), and greater rates in material processing are observed due to resonances. All these earlier works on heating and melting were carried out to investigate heating effects solely due to materials. The materials are typically processed with foreign supporting material or container, and the heating dynamics may depend on the complex interaction between the food materials and support.

The foreign supporting materials, such as ceramics (Al_2O_3, SiC), may play critical role on focusing microwaves within samples. Ceramic supports may be used for selective or controlled heating based on the properties such as Al_2O_3 is transparent for microwaves and SiC absorbs microwaves considerably. Therefore, optimal selection of ceramics toward the enhanced or efficient heating of the samples would be useful in microwave assisted processing. Earlier studies on microwave heating of ceramic materials show that Al_2O_3 absorbs less power than that in SiC resulting in greater heating in SiC (Chatterjee et al., 1998). One of the reasons to use ceramic in microwave heating is that the ceramic can withstand high-temperature. In addition, the temperature profile within the ceramic materials is uniform due to higher thermal conductivity, and these materials may be perfect choices to be used as supports.

Recently, Basak and Priya (2005) studied microwave heating of water (high dielectric loss) and oil (low dielectric loss) with ceramic supports (Al_2O_3 and SiC). It has been observed that either Al_2O_3 or SiC may be preferred for heating oil and water. These supports play critical role on enhanced heating of water and oil and efficient heating procedure also avoids thermal runaway. These studies provide suitable guideline on heating pure substances with ceramic supports. The microwave heating of food substances may involve processing of multiphase and multilayered samples in presence of ceramic supports. The complex interaction between multilayered food substances and ceramic support may be important to determine the efficient heating strategies, and such studies are yet to appear in literature.

Current work attempts to analyze the efficient heating strategies in presence of resonance or maxima in power within beef-oil layered samples with ceramic supports. The beef-oil layered sample may be used in food processing where the high lossy substance (beef) is thermally treated with a low lossy substance (oil). The microwave heating studies would be carried out to analyze the effect of various oil thicknesses and ceramic supports. The electric field and microwave power distributions are obtained via solving the Maxwell's equations for multilayered samples. The temperature distributions are obtained by solving the energy balance equation with a heat generation term due to microwave power absorption. The thermal characteristics and power distributions within the beef samples are investigated for various thicknesses of oil layer and ceramic supports. The heating studies were carried out for various cases such as oil layer or ceramic support is directly exposed to microwaves, beef layer is directly exposed to microwaves, and both oil layer/support and beef layer are exposed to microwaves. The optimal heating of layered samples has been highlighted based on runaway heating effects, beef-oil-ceramic support assembly and distributed microwave incidences.

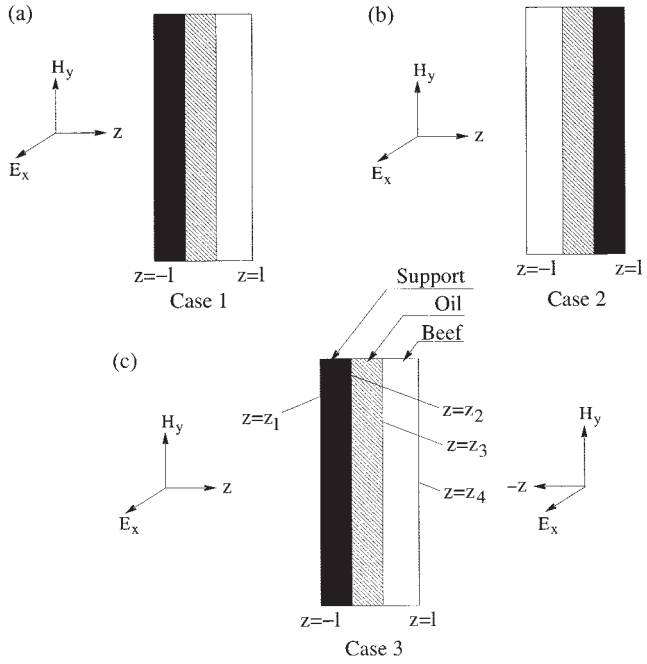

Figure 1. Multilayered sample exposed to plane electromagnetic waves for (a) Case 1: one side incidence (b) Case 2: one-side incidence, and (c) Case 3: both sides incidence.

Various layers and interface positions are shown in Figure 1 (c).

Theory

Electric field and power evaluations in multilayered systems

During microwave heating, the electric field propagates through the entire material. The microwave incidence may be at one side or both the sides as shown in Figures 1. The multilayered material may consist of beef, oil and/or ceramic materials. Note that the oil layer is directly attached with the support for all cases. Oil is generally used as an auxiliary cooking material and beef-oil slab represents the food composite typically used in food industry.

We assume that the sample thickness is much smaller compared to the lateral dimensions, and, hence, 1-D slab is a reasonable representation for the material-ceramics assembly. Similar modeling assumption can be found in earlier literatures (Basak and Ayappa, 1997; Basak, 2003; Basak, 2004a; Basak and Priya, 2005). Microwaves are assumed to be uniform plane

waves, and the wave propagation due to uniform electric field E_x, given by Maxwell's equation is

$$\frac{d^2E_x}{dz^2} + k^2E_x = 0 \tag{1}$$

where E_x lies in $x - y$ plane and varies only in the direction of propagation, z axis. In Eq. 1, $k = (\omega/c)\sqrt{\kappa' + i\kappa''}$ is the propagation constant which depends on the dielectric constant, κ' and the dielectric loss, κ'', $\omega = 2\pi f$, where f is the frequency of the electromagnetic wave, and c is the velocity of light. In a n multilayered sample the electric field for the l^{th} layer obtained from Eq. 1 is

$$\frac{d^2E_{x,l}}{dz^2} + k_l^2E_{x,l} = 0 \tag{2}$$

where $z_{l-1} \le z \le z_l$ and $l = 1 \cdots n$. We assume each layer has constant dielectric properties and hence, the general solution to Eq. 2 represented as a linear combination of transmitted and reflected waves propagating in opposite directions is

$$\begin{array}{lll} E_{x,1} = & E_{t,1}e^{ik_1z} + E_{r,1}e^{-ik_1z} & \text{First layer} \\ E_{x,l} = & E_{t,l}e^{ik_lz} + E_{r,l}e^{-ik_lz} & \text{Intermediate layers} \\ & & l = 2. \ . \ .n-1 \\ E_{x,n} = & E_{t,n}e^{ik_nz} + E_{r,n}e^{-ik_nz}, & n^{\text{th}} \text{ layer} \end{array} \tag{3}$$

where $E_{t,l}$ and $E_{r,l}$ are the coefficients due to transmission and reflection respectively. The boundary conditions at the interface are

$$\left.\begin{array}{l} E_{x,l-1} = E_{x,l} \\ \dfrac{dE_{x,l-1}}{dz} = \dfrac{dE_{x,l}}{dz} \end{array}\right\} \begin{array}{l} l = 2. \ . \ .n \\ z = z_1. \ . \ .z_{n-1} \end{array} \tag{4}$$

Here $z_1, z_2 \cdots z_{n-1}$ denote various interface positions as seen in Figure 1c. The interface conditions and the general solutions, are used to obtain the coefficients, $E_{t,l}$ and $E_{r,l}$ via solving the set of algebraic equations. As the incident field intensities from the left and right are known, that is, $E_{t,1} = E_L$ and $E_{r,n} = E_R$, the corresponding equations are solved for the remaining $2n$–2 coefficients. Note that, E_L and E_R may be obtained from incident intensities where the intensity, I_0 is related with the electric field, E_0 as $I_0 = (1/2)c\varepsilon_0E_0^2$, where ε_0 is free space permittivity. For the l^{th} layer, the transmitted and reflected waves are

$$\begin{aligned} E_{x,l}^t &= E_{t,l}e^{ik_lz} = A_{x,l}^t e^{i\delta_{x,l}^t} \\ E_{x,l}^r &= E_{r,l}e^{-ik_lz} = A_{x,l}^r e^{i\delta_{x,l}^r} \end{aligned} \tag{5}$$

with corresponding amplitudes

$$\begin{aligned} A_{x,l}^t &= \sqrt{E_{x,l}^t E_{x,l}^t{}^*} \\ A_{x,l}^r &= \sqrt{E_{x,l}^r E_{x,l}^r{}^*} \end{aligned} \tag{6}$$

and the phase states

$$\begin{aligned} \delta_{x,l}^t &= \tan^{-1}\left[\frac{\text{Im}(E_{x,l}^t)}{\text{Re}(E_{x,l}^t)}\right] \\ \delta_{x,l}^r &= \tan^{-1}\left[\frac{\text{Im}(E_{x,l}^r)}{\text{Re}(E_{x,l}^r)}\right] \end{aligned} \tag{7}$$

where the superscript, "*" in Eq. 6 denotes the complex conjugate. For a stationary wave in the l^{th} layer, the amplitude is given by

$$A_{x,l} = \sqrt{E_{x,l}E_{x,l}^*} \tag{8}$$

and the difference in phase angle is given by

$$\delta_{x,l} = \delta_{x,l}^t - \delta_{x,l}^r \tag{9}$$

where the quantities $E_{x,l}$ and $E_{x,l}^*$ appeared in Eq. 8 are evaluated using Eqs. 3 and 5. At the resonance, the difference in phase angle is zero, that is, $\delta_{x,l} = 0$. The above analysis on the solution of electric fields are based on the assumptions such as the dielectric properties of various layers are invariant during the entire heating and the reflected waves from materials as well as supports do not affect the power sources (that is, magnetron).

The absorbed power in l^{th} layer, obtained from Poynting vector theorem is

$$q_l(z) = \frac{1}{2}\,\omega\varepsilon_0\kappa''E_{x,l}(z)\,E_{x,l}^*(z) \tag{10}$$

The average power obtained by integrating the power across the multilayered slab is

$$q_{av} = \frac{1}{2L}\int_{-L}^{+L} q_l(z)dz \approx \frac{1}{n}\sum_{i=1}^{n} q_l(z_i) \tag{11}$$

Here $-L$ and L denote the left and right faces of the slab, respectively, and $q_l(z)$ denotes the power as a function of z, where z may be measured from the left edge of the multilayered slab. Note that, $2L$ is the thickness of the entire slab consisting of beef, oil and supports. We will denote L_s as the thickness of the beef sample and L' as the total thickness of the support and oil layer such that $2L = L_s + L'$. The average power for a beef sample of thickness L_s is

$$q_{av,b} = \frac{1}{n}\sum_{i=1}^{n} q_l(z_i), \quad \text{for } 0 \le z_i \le L_s \tag{12}$$

Microwave heating and energy transport

The material is assumed to have constant thermal properties throughout the heating process. The material is also assumed to be at the same phase and the natural convection within the

Table 1. The Thermal and Dielectric Properties are Given for Water, Oil, Raw Beef, Al_2O_3 and SiC*

Material Property	Water	Oil	Raw Beef	Al_2O_3	SiC
heat capacity, C_p (J kg^{-1} °K^{-1})	4190	2000	2510	1046	3300
thermal conductivity, k (W m^{-1} °K^{-1})	0.609	0.168	0.491	26	40
density, ρ (kg m^{-3})	1000	900	1070	3750	3100
dielectric constant (2450 MHz), κ'	78.1	2.8	43	10.8	26.66
dielectric loss (2450 MHz), κ''	10.44	0.15	15	0.1566	27.99

*(Chatterjee et al., 1998; Basak and Priya, 2005).

material (beef) and oil layer may be neglected. The heat transport due to microwave radiation is governed by energy balance equation. The energy balance equation due to microwave assisted heat source is

$$\rho c_p \frac{\partial T}{\partial t} = k \frac{\partial^2 T}{\partial z^2} + q(z) \tag{13}$$

where ρ is the density, c_p is the specific heat, k is the thermal conductivity and the volumetric heat source, $q(z)$ is defined in a similar manner as in Eq. 10. In a n multilayered sample, the energy balance equation for the l^{th} layer obtained from Eq. 13 is

$$(\rho c_p)_l \frac{\partial T_l}{\partial t} = k_l \frac{\partial^2 T_l}{\partial z^2} + q_l(z) \quad l = 1 \ldots n \tag{14}$$

The initial condition is

$$T_l = T_0 \tag{15}$$

and the boundary conditions are

$$k_1 \frac{\partial T_1}{\partial z} = h(T_1 - T_\infty) \quad z = z_1 \tag{16}$$

and

$$-k_{n-1} \frac{\partial T_{n-1}}{\partial z} = h(T_{n-1} - T_\infty) \quad z = z_{n-1}, \tag{17}$$

The interface conditions between ceramic-material are

$$\left.\begin{aligned} T_l &= T_{l+1} \\ k_l \frac{\partial T_l}{\partial z} &= k_{l+1} \frac{\partial T_{l+1}}{\partial z} \end{aligned}\right\} \begin{aligned} l &= 2 \ldots n-2 \\ z &= z_2 \ldots z_{n-2} \end{aligned} \tag{18}$$

The wave propagation equation for a particular medium (ceramic/material) is given in Eq. 2. As microwave power, $q_l(z)$ is a function of electric field as seen in Eq. 10, hence, a functional representation of electric field is necessary to solve the energy balance equation (Eq. 14). The evaluation of functional form of electric field may be difficult for a multilayered sample, and we are unaware of such a solution till date. Alternatively, the energy balance and wave equations (Eqs. 14 and 2) can be solved numerically as discussed in earlier works (Basak, 2003; Basak and Priya, 2005).

Solution strategy and parameters

The energy balance equation and the electric field equations with the appropriate boundary conditions are solved using Galerkin finite element method. The interface conditions for energy balance and electric field equations due to multiple phases are automatically satisfied via an interface element common to two phases. At the interface node, the field variable and fluxes are continuous as discussed by Ayappa et al. (1991). To discretize the time domain, Crank-Nicholson method is used, and the nonlinear residual equations are solved using a Newton Raphson Method. Due to the lack of a good initial guess to begin the Newton scheme, a small time step $\Delta t = 1 \times 10^{-4}$ s was used at the first time step. Unless specified otherwise $\Delta t = 0.1$ s was used for subsequent steps and typically 25–50 quadratic elements were used. It was found that the maximum difference for the values of the unknowns at the nodes was less than 1% when the values were compared for 25 and 50 elements. Similarly the maximum difference was less than 1% when the results were compared for $\Delta t = 0.05$ s and 0.1 s.

The dielectric and thermal properties are obtained from Table 1. Note that dielectric properties correspond to MW frequency 2450 MHz. The microwave incidence may be distributed via one source and both the sources at the sides as seen in Figure 1. In all cases, the sample is exposed to the total microwave radiation of intensity 3 W · cm^{-2}. The composite dielectric consisting of beef-oil layers with/without any support and the heating strategy has been investigated for oil layer followed by beef layer (case 1), beef layer followed by oil layer (case 2), and oil-beef layers exposed to microwaves at the both the sides (case 3). For cases 1 and 2, the microwaves are incident at the left face only. The heat-transfer coefficient at the outer faces is maintained at 2 W · m^{-2} · K^{-1}. The temperature of the sample and the support is 300 K at $t = 0$ s. The thickness of the sample varies between 0.1–10 cm and the oil layer thickness varies within 0.1–2 cm.

Results and Discussion

Microwave power and temperature distributions without any support: one-side incidence

The processing of beef-oil layered composite substance has been investigated for enhanced heating rates corresponding to greater microwave power absorption. The greater microwave power absorption or maxima in power, also termed as resonances, occurs for specific length scales of the layered composite. The resonances can be best illustrated by average power vs. sample thickness diagram where the two consecutive power maxima are referred as R_1 and R_2 modes. The results primarily highlight the microwave power absorption in beef samples.

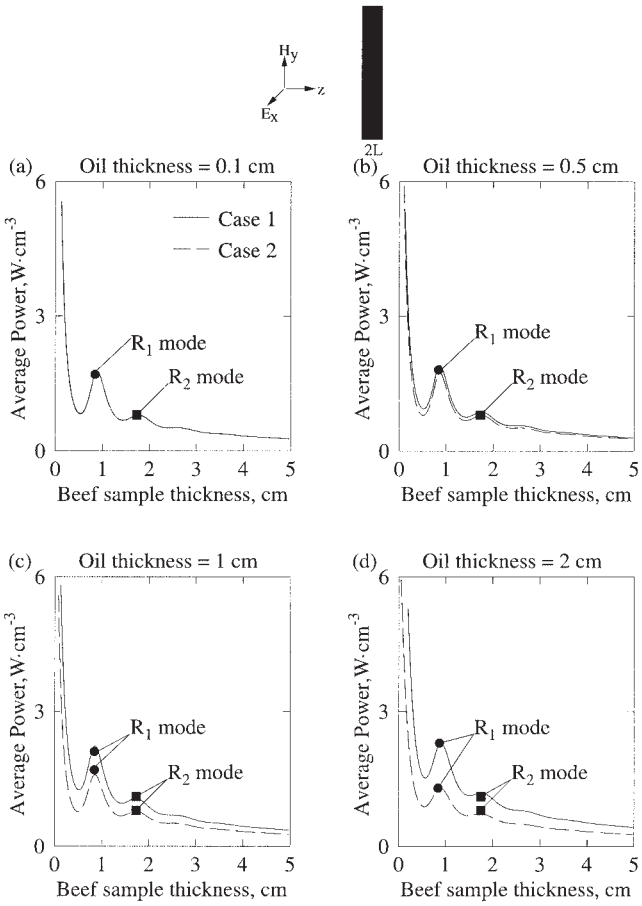

Figure 2. Average power in beef samples (W · cm^{-3}) vs. sample thickness (cm) for case 1 and case 2 in absence of support with various oil thicknesses: (a) l_o = 0.1 cm, (b) l_o = 0.5 cm, (c) l_o = 1 cm, and (d) l_o = 2 cm exposed to microwaves at one face. f = 2,450 MHz, I_0 = 3 W · cm^{-2}.

The filled circle denotes R_1 mode and the filled rectangle denotes R_2 mode of resonances. The average power for case 1 during R_1 and R_2 modes is larger for greater oil thicknesses ($l_o \geq 1$ cm).

Figures 2 illustrates the average power distributions vs. beef sample thickness for case 1 and case 2 with various oil thicknesses (0.1 cm, 0.5 cm, 1 cm and 2 cm). Note that, the circles indicate R_1 mode and boxes indicate R_2 mode. During one side incidence, the average power for a sample without any support exhibits maxima at $L_s = 0.5\lambda_m$ and λ_m during R_1 and R_2 modes, respectively. Note that, the wavelengths (λ_m) for oil and raw beef samples are 7.3 cm and 1.84 cm, respectively. The average power vs. sample thickness diagram indicates that the beef sample thickness (L_s) corresponding to R_1 or R_2 mode remains identical for cases 1 and 2 at specific oil thickness. Note that, the beef sample thickness (L_s) corresponding to R_1 mode are 0.89 cm, 0.87 cm, 0.85 cm and 0.89 cm for oil thicknesses 0.1 cm, 0.5 cm, 1 cm and 2 cm, respectively during cases 1 and 2 (see Figures 2a–d). Although occurrence of resonances within beef samples for specific oil thickness does not vary from case 1 to case 2, it is interesting to observe that the average power corresponding to case 1 is greater than that for case 2 at a fixed oil thickness with $l_o \geq 0.5$ cm. It is also interesting to note that, the average power absorption in beef samples is higher for large oil thicknesses with case 1 whereas higher average power is found to occur for small oil thicknesses with case 2, corresponding to fixed resonance mode (R_1 or R_2).

The efficient thermal processing of beef sample depends on the role of oil thickness and complex dielectric interaction between support, oil and beef samples. The detailed analysis on MW power characteristics and electric field distributions at various resonance modes would be useful to understand the interference of waves and the critical role of the specific ceramic support.

Figures 3 illustrates the amplitude, power and temperature distributions for case 1 during R_1 mode. Various distributions are shown for l_o = 0.1, 0.5, 1 and 2 cm. For all oil thicknesses, it has been observed that the amplitude of transmitted wave is a decreasing function of the distance whereas the amplitude of the reflected wave is an increasing function of distance within the beef sample. It is interesting to note that, there is a significant jump in the amplitudes of transmitted and reflected waves within the oil thickness. It has been observed that, the amplitudes of both transmitted and reflected fields

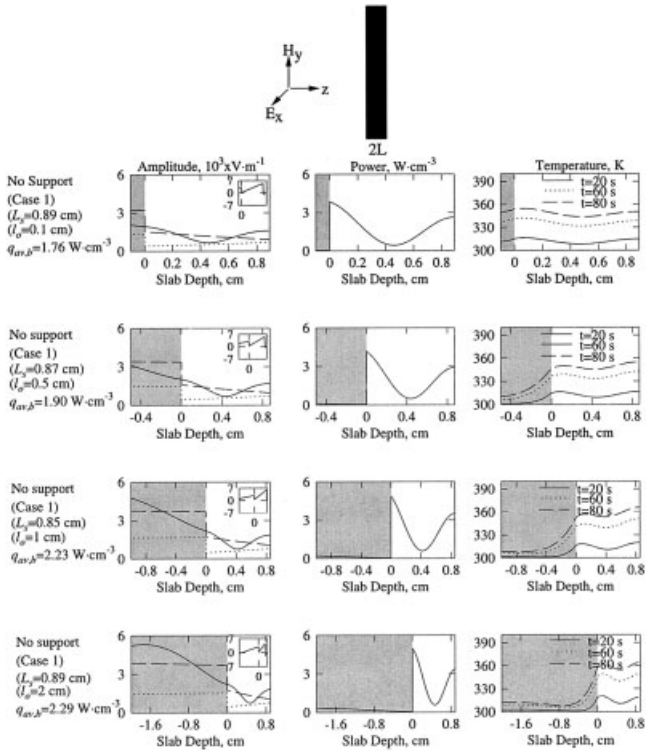

Figure 3. Amplitudes of electric field ($A_{x,l}$, $A^t_{x,l}$, $A^r_{x,l}$), power distributions and temperature profiles for case 1 with oil layer exposed to microwaves from the left face during R_1 mode in absence of any support.

The shaded regime denotes the oil layer. Note that, various oil thicknesses are l_o = 0.1 cm, 0.5 cm, 1 cm, and 2 cm; — — —, transmitted wave; . . . . . , reflected wave; —, stationary wave. The inset shows phase difference ($\delta_{x,l}$) vs. z. f = 2,450 MHz, I_0 = 3 W · cm^{-2}. Greater heating rates are observed for larger oil thicknesses ($l_o \geq 1$ cm).

within the oil sample are almost constant and larger than that in the beef sample. Although the amplitudes of the electric field are larger in oil sample, the power absorption within beef sample is greater than that in oil samples due to high dielectric loss of beef sample. It is also observed that, the amplitude of transmitted wave is increased in the oil layer for larger oil thicknesses. Therefore, the power absorption at the oil-beef interface is also increased with the thickness of oil layer. Note that, the average powers in beef sample ($q_{av,b}$) are 1.76 W · cm^{-3}, 1.90 W · cm^{-3}, 2.23 W · cm^{-3}, and 2.29 W · cm^{-3} for l_o = 0.1 cm, 0.5 cm, 1 cm and 2 cm, respectively. Similar qualitative features in microwave power distribution within the beef sample have also been observed for R_2 mode.

The spatial resonances of microwave power are illustrated via the inset plot which shows the distribution of phase angle vs. slab depth with the zero phase difference signifying the constructive interference which also represents local resonance. For all the cases, it has been observed that the two maxima in power or resonances occur at both the ends of the beef sample irrespective of various oil thickness. Temperature distributions within the samples are illustrated by spatial temperature vs. sample thickness diagram as seen in Figures 3. The temperature distribution within the beef sample qualitatively follow the power distribution during initial stages, and the greater temperature at the unexposed face of the beef sample is observed at the later stages due to the almost insulated situation at the right end (h = 2 W · m^{-2} · K^{-1}). The temperature distribution is quite stiff within oil sample due to lower thermal conductivity of oil (see Table 1). Here the temperatures (K) are shown at 20 s, 60 s, and 80 s. During 80 s, the temperature within the beef sample varies within 343–354 K, 346–354 K, 353–365 K and 354–364 K for l_o = 0.1 cm, 0.5 cm, 1 cm and 2 cm, respectively. Note that, the greater heating at the unexposed end of the beef sample may cause the thermal runaway. Consequently, the uniform heating within the beef sample may not be observed for larger oil thicknesses as seen in Figures 3.

Figures 4 illustrates the amplitude, power and temperature distributions for case 2 during R_1 mode with various oil thicknesses: l_o = 0.1, 0.5, 1 and 2 cm. Similar to Figures 3, it has been observed that the amplitude of transmitted wave is a decreasing function of the distance within the beef sample, and the amplitude of the reflected wave is an increasing function of the distance. The qualitative features on distributions of amplitudes of traveling waves in the oil layer are similar to that in case 1; however, the amplitudes of both the transmitted and reflected waves are smaller in case 2 (Figures 4). It is observed that the amplitude of the reflected wave in the oil layer is found to be decreased with the thickness of oil layer. As a result, the intensity of stationary wave in the oil layer would be smaller than that with case 1. In addition, the distribution of amplitude of the stationary electric field in the beef layer is found to be decreased with the thickness of oil layer. Similar to Figures 3, it has been observed that the maxima in power (resonance) occurs at both the ends of the beef sample. It is observed that the average power is 1.3 W · cm^{-3} for l_o = 2 cm, whereas the average power corresponding to l_o = 0.1 cm is 1.75 W · cm^{-3}. In contrast, the average power in the beef sample is increased with the thickness of oil layer as seen in case 1.

The temperature distributions within the samples illustrate that the maxima in temperature occurs at the exposed face, whereas for case 1 the maxima in temperature was found at the

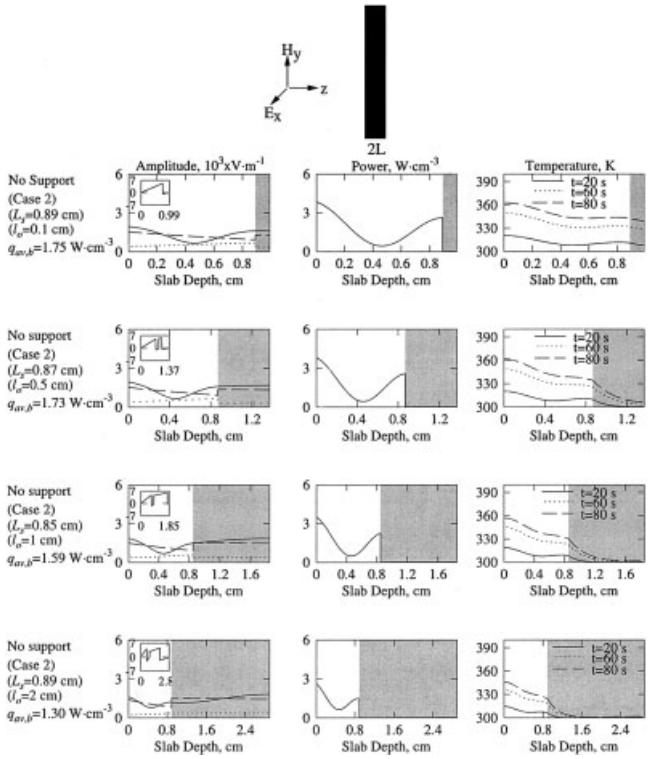

Figure 4. Amplitudes of electric field ($A_{x,l}$, $A^t_{x,l}$, $A^r_{x,l}$), power distributions and temperature profiles for case 2 with beef layer exposed to microwaves from the left face during R_1 mode in absence of any support.

The shaded regime denotes the oil layer. Note that, various oil thicknesses are l_o = 0.1 cm, 0.5 cm, 1 cm, and 2 cm; — — —, transmitted wave; . . . . . , reflected wave; —, stationary wave. The inset shows phase difference ($\delta_{x,l}$) vs. z. f = 2450 MHz, I_0 = 3 W · cm^{-2}. Greater heating rates are observed near the exposed face for smaller oil thicknesses ($l_o \leq$ 1 cm).

unexposed face within the beef layer. It is interesting to note that, for specific oil thicknesses the maxima in temperature with case 2 is smaller than that with case 1 due to less power deposition in case 2. In addition, the temperature of the oil layer is also smaller than that with case 1. Note that, during 80 s, the temperature variations in the beef layer are within 342–362 K, 334–361 K, 330–357 K and 324–346 K for l_o = 0.1, 0.5, 1 and 2 cm, respectively. It may also be noted that, the maxima in temperature is decreased with the increased thickness of oil layer which is in contrast with the case 1. The greater thickness of oil layer with case 2 may be sometime preferable due to less runaway heating situations whereas case 1 with all ranges of thickness would cause greater average power or average heating rate for beef layer.

We have also carried out simulations for R_2 modes with cases 1 and 2, and similar qualitative features have been observed (figures not shown). The runaway heating effect as seen in Figures 3 and 4 may be quantified via the difference in maximum and minimum temperature in the beef sample (ΔT_b).

Figures 5 illustrates the variation of temperature difference (ΔT_b) with time for cases 1 and 2 with various oil thicknesses.

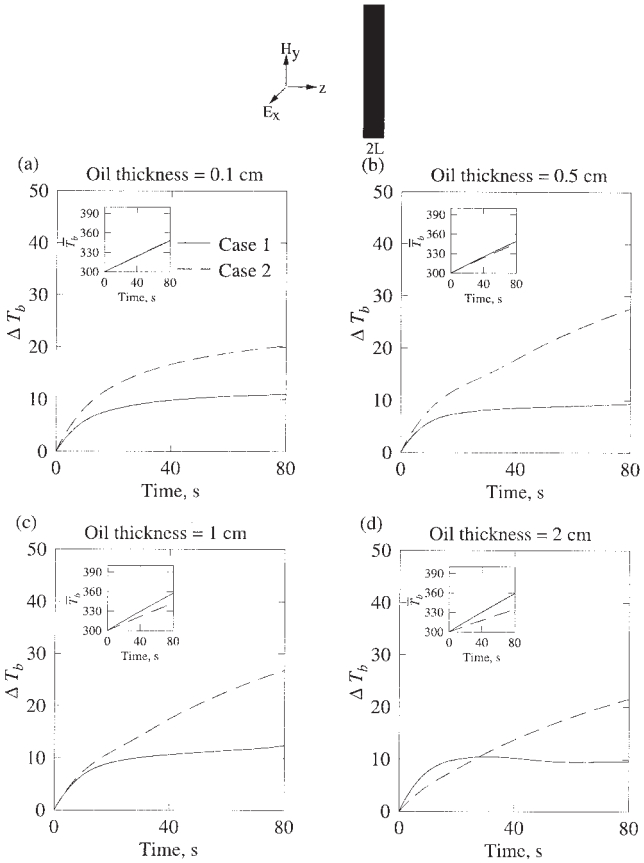

Figure 5. The temperature difference in beef samples, ΔT_b (K) vs. time (s) for case 1 and case 2 in absence of any support for samples incident with microwaves at one face during R_1 mode for (a) l_o = 0.1 cm, (b) l_o = 0.5 cm, (c) l_o = 1 cm, and (d) l_o = 2 cm.

The insets denote the average temperature, $\bar{T}_b$ (K) vs. time (s). Case 1 corresponds to less thermal runaway for all thicknesses of oil.

The insets show the average temperature ($\bar{T}_b$) vs. time plot where the slope of that plot denotes the average heating rate which is directly proportional to the MW power absorption. Figure 5a illustrates the distributions for $l_o = 0.1$ cm, and it is observed that for both the cases the temperature difference (ΔT_b) shows a steady value at the later stages of heating. During initial stages of heating ($t \leq 10$ s), the temperature difference is increasing rapidly to illustrate the greater heating effects due to exposition of microwaves of the sample which is initially kept at 300 K. It is observed that ΔT_b is around 11 K for case 1 and 20 K for case 2 at 80 s (Figure 5a). Note that, the average heating rate is identical as seen from the inset plot for both cases 1 and 2 with $\bar{T}_b$ being 348 K at 80 s. Figures 5b–d illustrate the distributions for $l_o = 0.5$ cm, 1 cm and 2 cm, respectively. It is observed that the runaway heating situation is more pronounced with case 2 for $l_o = 0.5$ and 1 cms. The temperature difference (ΔT_b) is 27 K and 26 K for $l_o = 0.5$ cm and 1 cm, respectively, with case 2, whereas $\Delta T_b = 21$ K for $l_o = 2$ cm with case 2. It may also be noted that the heating rates are identical for cases 1 and 2 with $l_o = 0.1$ cm and 0.5 cm, whereas the rate is larger with case 1 for $l_o = 1$ cm and 2 cm. For all the oil thicknesses, the temperature difference (ΔT_b) is maintained at 10–14 K with case 1 during 80 s. Therefore, case 1 may be a favored configuration to heat the beef-oil composite dielectric due to smaller runaway heating effects and optimal oil thickness may be chosen based on the competition between the thermal runaway and average heating rate.

Microwave power and temperature distributions with ceramic supports: one-side incidence

Figures 6a–d illustrate the average power distribution vs. beef sample thickness in presence of ceramic supports (Al_2O_3 and SiC) for cases 1 and 2 with various oil thicknesses. For all cases, the supports are attached with the oil layer. We have assumed a thickness of support being 0.2 cm for all test cases. Note that, we assumed smaller thickness of support and influ-

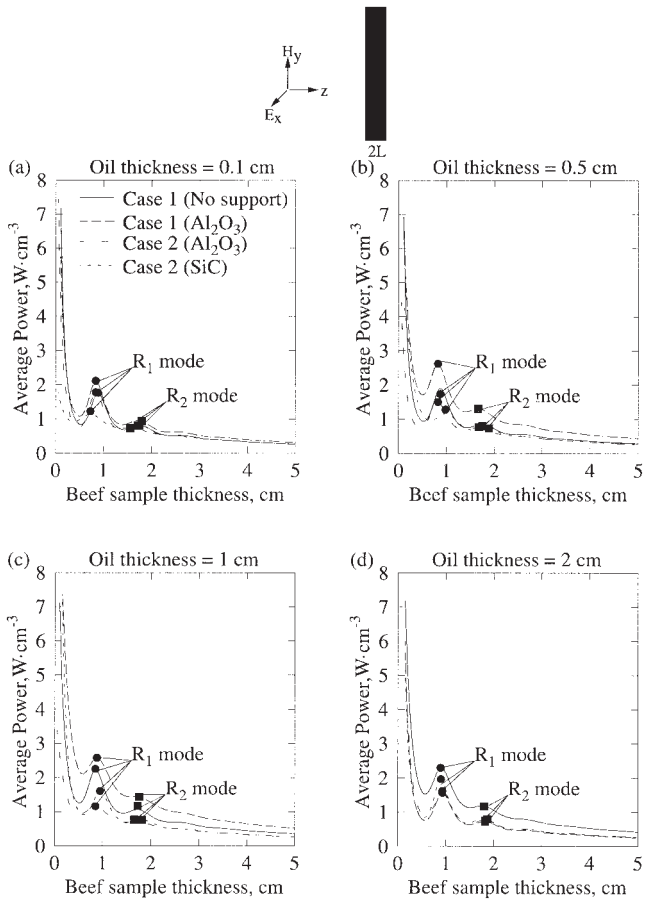

Figure 6. Average power in beef samples ($W \cdot cm^{-3}$) vs. sample thickness (cm) for case 1 and case 2 in the presence of Alumina (Al_2O_3) and SiC supports with various oil thicknesses: (a) l_o = 0.1 cm, (b) l_o = 0.5 cm, (c) l_o = 1 cm, and (d) l_o = 2 cm exposed to microwaves at one face.

The ceramic support thickness = 0.2 cm. f = 2450 MHz, $I_0 = 3\ W \cdot cm^{-2}$. The filled circle denotes R_1 mode and the filled rectangle denotes R_2 mode of resonances. The average power for case 1 with Alumina support during R_1 and R_2 modes is larger for smaller oil thicknesses ($l_o \leq 1$ cm).

ence of various thicknesses of support on microwave heating of materials may not be important for current work.

The efficient heating due to microwaves may be either at R_1 or R_2 mode and the maxima of power within the beef sample corresponds to specific sample thicknesses. The maxima in power within the sample for various cases would vary with oil thicknesses and ceramic supports. Note that, the average power is enhanced for case 1 with Al_2O_3 support and $l_o \leq 1$ cm. It has been observed that $q_{av,b} = 1.76\ \mathrm{W \cdot cm^{-3}}$ for case 1 with no support, $q_{av,b} = 2.1\ \mathrm{W \cdot cm^{-3}}$ for case 1 with Al_2O_3 support, $q_{av,b} = 1.77\ \mathrm{W \cdot cm^{-3}}$ for case 2 with Al_2O_3 support, and $q_{av,b} = 1.14\ \mathrm{W \cdot cm^{-3}}$ for case 2 with SiC support for $l_o = 0.1$ cm (see Figure 6a). The sample thickness (L_s) corresponding to a specific resonance mode and specific oil thickness for cases 1 and 2, remains almost unaffected by Al_2O_3 supports and the sample thickness (L_s) is smaller with the SiC support. These features are observed for smaller oil thicknesses ($l_o \leq 1$ cm). For larger oil thicknesses, the sample thickness (L_s) for a specific resonance mode remains unaffected by either Al_2O_3 or SiC support. Similar to the cases without supports (as discussed in the previous section), the case 1 with supports corresponds to greater average power than that for case 2 with supports for smaller oil thicknesses ($l_o \leq 1$ cm). For $l_o = 2$ cm, it is observed that average power for case 2 with SiC support is larger than that for cases 1 and 2 with Alumina support. Note that, $q_{av,b} = 2.29\ \mathrm{W \cdot cm^{-3}}$ for case 1 with no support, $q_{av,b} = 1.55\ \mathrm{W \cdot cm^{-3}}$ with Al_2O_3 support, $q_{av,b} = 1.61\ \mathrm{W \cdot cm^{-3}}$ for case 2 with Al_2O_3 support, $q_{av,b} = 1.96\ \mathrm{W \cdot cm^{-3}}$ for case 2 with SiC support for $l_o = 2$ cm as seen in Figure 6d. Note that, Alumina support reduces microwave power absorption within the beef sample for greater oil thicknesses ($l_0 \geq 1$ cm) specially for case 1.

Figures 7 illustrates the amplitude, power and temperature distributions for cases 1 and 2 with ceramic supports (Al_2O_3 and SiC) during R_1 mode for one-side incidence corresponding to $l_o = 0.1$ cm. For cases 1 and 2, the sample thicknesses (L_s) are almost identical with Al_2O_3 support whereas the sample thickness is smaller with SiC support. Similar to the previous case without any support, it is also observed that, for cases 1 and 2 with Al_2O_3 support the amplitude of the transmitted wave is a decreasing function of distance, whereas the amplitude of reflected wave is an increasing function of distance within the beef sample. It is interesting to observe that there are significant jumps in the amplitudes of the transmitted and reflected waves at the interfaces of beef-oil and oil-ceramic layers. Note that, the amplitudes of the traveling and stationary waves within the oil and beef layers are enhanced due to the presence of Al_2O_3 support specially for case 1. Although Al_2O_3 support for case 2 causes small enhancement of the spatial power distribution, but SiC support corresponds to smaller power deposition throughout the beef sample. Note that, due to smaller dielectric loss of the Al_2O_3 support, the microwave power absorption is quite small within the support. Therefore Al_2O_3 supports can be efficiently used due to the less power consumption. The role of SiC support may be illustrated with a fact that more transmission and reflection within the support may decrease the amplitudes of traveling waves within the sample. Therefore, SiC support is preferred to keep at the unexposed face of the sample.

The insets show the difference in phase angle vs. distance within the slab. The resonances or maxima in power occur on

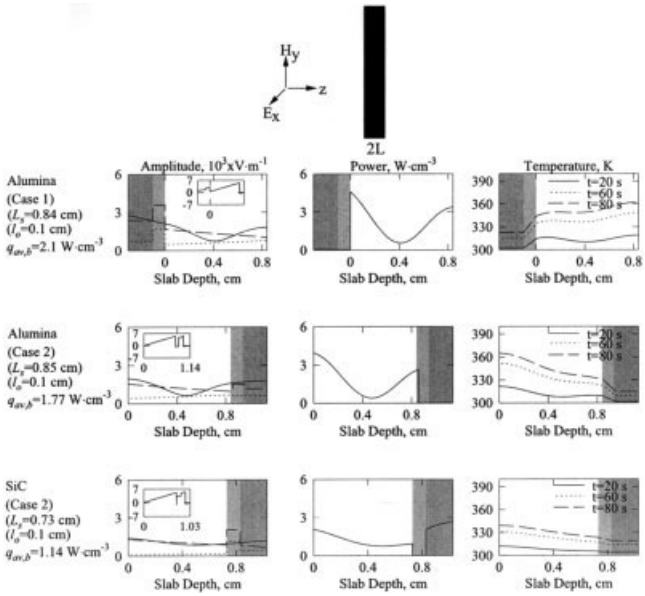

Figure 7. Amplitudes of electric field ($A_{x,l}$, $A^t_{x,l}$, $A^r_{x,l}$), power distributions and temperature profiles for cases 1 and 2 with Alumina (Al_2O_3), and SiC supports where the samples exposed to microwaves from the left face during R_1 mode.

The darker shaded regime denotes the support and the lighter shade denotes the oil layer. The thickness of the oil layer is 0.1 cm and the thickness of support is 0.2 cm. — — —, transmitted wave; . . . . . , reflected wave; —, stationary wave. The inset shows phase difference ($\delta_{x,l}$) vs. z. f = 2,450 MHz, $I_0 = 3\ \mathrm{W \cdot cm^{-2}}$. Greater heating rates are observed near the exposed face for case 2 with Alumina support.

both faces of the beef sample except the beef-oil samples attached with SiC support, and it is observed that the smaller power deposition occurs at the unexposed end of beef sample attached with oil-ceramic layer for case 2.

The temperature distributions within the samples are illustrated by spatial temperature vs. sample thickness diagram in Figures 7. The larger temperature at the unexposed face for the case 1 and at the exposed face for case 2 of the beef sample with Al_2O_3 is observed at the later stages. It is also observed that the temperature distribution is quite stiff within oil sample due to lower thermal conductivity of oil whereas the temperature distribution is uniform within the ceramic support due to higher values of thermal conductivity. Therefore, the largest temperature is found to occur at the face which is not attached with oil-ceramic layers. The temperatures are shown for 20 s, 60 s, and 80 s. During 80 s, the temperature in beef samples varies within 344–362 K, 329–364 K and 323–339 K for case 1 with Al_2O_3 support, case 2 with Al_2O_3 support and case 2 with SiC support, respectively. It is interesting to observe that Al_2O_3 support corresponds to larger heating rates. However, the runaway heating may occur due to Al_2O_3 supports whereas SiC support corresponding to lower heating rates may be preferred to avoid *hot spots* for heating highly lossy substances (beef).

Figures 8 illustrates the amplitude, power and temperature distributions for cases 1 and 2 with Al_2O_3 and SiC supports during R_1 mode for one side incidence corresponding to $l_o =$

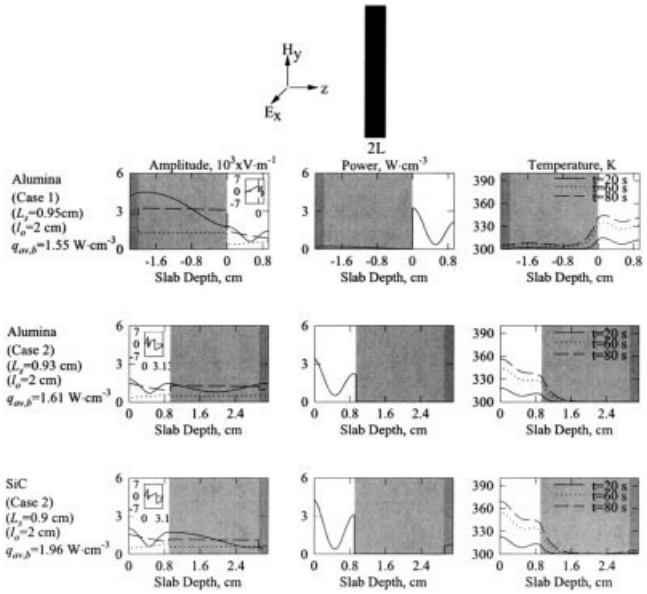

Figure 8. Amplitudes of electric field ($A_{x,l}$, $A^t_{x,l}$, $A^r_{x,l}$), power distributions and temperature profiles for cases 1 and 2 with Alumina (Al_2O_3) and SiC supports where the samples exposed to microwaves from the left face during R_1 mode.

The darker shaded regime denotes the support and the lighter shade denotes the oil layer. The thickness of the oil layer is 2 cm and the thickness of support is 0.2 cm. — — —, transmitted wave; . . . . . , reflected wave; —, stationary wave. The inset shows phase difference ($\delta_{x,l}$) vs. z. f = 2,450 MHz, I_0 = 3 W · cm^{-2}. Greater heating rates are observed near the exposed face for case 2 with both Alumina and SiC supports.

2 cm. Unlike for l_o = 0.1 cm, the sample thicknesses (L_s) are almost identical for cases 1 and 2 with Al_2O_3 and SiC supports. It is interesting to note that for l_o = 2 cm, the overall power absorption is small within the oil and ceramic layers for cases 1 and 2. The variations of amplitudes of traveling and stationary waves within beef-oil-ceramic layers are qualitatively similar to the previous case with l_o = 0.1 cm as seen in Figure 7. It is observed that, the overall amplitude distributions within the beef layer with Al_2O_3 support are smaller than that for beef layer with Al_2O_3 support for l_o = 0.1 cm with cases 1 and 2. In contrast, the amplitudes in the beef layer with SiC support are larger than that for beef layer with SiC support for l_o = 0.1 cm. The enhancement of amplitudes of fields in the beef layer results in greater average power for case 2 with SiC support (q_{av} = 1.96 W · cm^{-3}) for l_o = 2 cm, whereas the average powers are around 1.55 W · cm^{-3}, 1.61 W · cm^{-3} for Al_2O_3 support with cases 1 and 2, respectively. The insets illustrate that two maxima in amplitudes occur at both the faces of the beef samples for the cases with Al_2O_3 and SiC supports. In contrast, the power absorption in beef samples due to SiC support is low for l_o = 0.1 cm as only one maxima in amplitude of fields occurs at one of the faces.

The temperature distributions are shown at 20 s, 60 s, and 80 s. Note that during 80 s the temperature varies within 336–341 K for case 1 with Al_2O_3 support, 332–356 K for case 2 with Al_2O_3 support and 340–369 K for case 2 with SiC support. It is interesting to note that, the runaway heating situation occurs for cases 1 and 2 with Al_2O_3 and SiC supports. Unlike the previous case with l_o = 0.1 cm, SiC support does not offer any advantage to avoid runaway situation in heating samples with larger oil thicknesses.

Figures 9 illustrates the variation of temperature difference (ΔT_b) and average temperature ($\bar{T}_b$) within beef sample with time for cases 1 and 2 in presence of ceramic supports (Al_2O_3 and SiC) with various oil thicknesses. The insets show the average temperature ($\bar{T}_b$) vs. time plot where the slope denotes the heating rate. Figure 9a illustrates the temperature distribution for l_o = 0.1 cm. It is observed that case 1 with Al_2O_3 support and case 2 with SiC support correspond to less temperature difference than that for case 2 with Al_2O_3 support. During 80 s the temperature difference (ΔT_b) is around 18 K for case 1 with Al_2O_3 support and 15 K for case 2 with SiC support, whereas the temperature difference is 35 K for case 2 with Al_2O_3 support. It is interesting to observe that the heating rates for both the cases with Al_2O_3 support are almost same ($\bar{T}_b$ = 345–352 K) and case 2 with SiC support corresponds to smaller heating rate with less average temperature ($\bar{T}_b$ = 331 K) during 80 s.

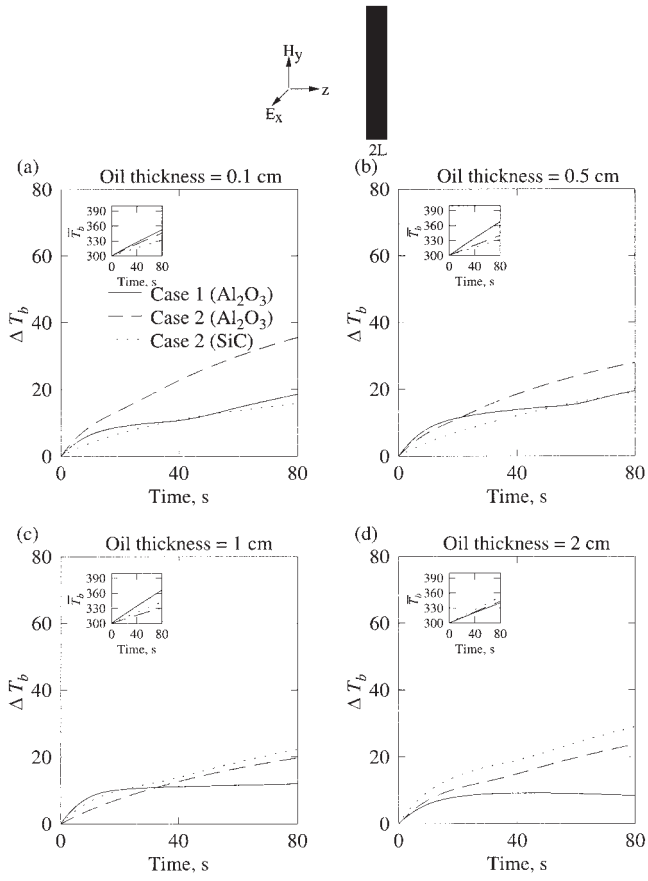

Figure 9. The temperature difference in beef samples, ΔT_b (K) vs. time (s) for case 1 and case 2 in presence of supports with samples incident with microwaves at one face during R_1 mode for (a) l_o = 0.1 cm, (b) l_o = 0.5 cm, (c) l_o = 1 cm, and (d) l_o = 2 cm.

The insets denote the average temperature, $\overline{T_b}$ (K) vs. time (s). Case 1 with Alumina (Al_2O_3) support corresponds to less thermal runaway for larger thicknesses of oil ($l_o \geq$ 1 cm).

Figures 9b–d illustrate the temperature distributions for oil thicknesses (l_o) 0.5 cm, 1 cm and 2 cm, respectively. It is interesting to observe that the temperature difference (ΔT_b) is smaller for larger oil thicknesses. For $l_o = 0.5$ cm, it is also observed that the temperature difference (ΔT_b) is lesser for case 1 with Al_2O_3 support, and case 2 with SiC support whereas for $l_o \geq 1$ cm the temperature difference is found to be lesser for case 1 with Al_2O_3 support only. For $l_o = 2$ cm, we have found that during 80 s the temperature difference is smaller ($\Delta T_b = 8$ K) for case 1 with Al_2O_3 support whereas $\Delta T_b = 23$ K and 28 K for cases 2 with Al_2O_3 and SiC supports, respectively. It is also observed that the heating rates are identical for cases 1 and 2 with Al_2O_3 supports and the heating rate is found to be slightly higher with SiC support (Figure 9d). Overall, case 1 with Al_2O_3 support may be a favored configuration to heat the beef-oil composite due to smaller runaway heating effects, and SiC support may also be preferred for less runaway heating effects for $l_o \leq 0.5$ cm.

Efficient heating due to microwaves: one side vs. both sides

This section deals with microwave heating of beef-oil layers for case 3 with supports attached to the oil layer. Similar to previous sections, the thickness of support is assumed to be 0.2 cm for all test cases. Note that, case 3 corresponds to both sides incidence where the total intensity of incident microwaves is 3 $W \cdot cm^{-2}$. Various combinations of microwaves incidence at both sides correspond to types I, II, III and IV and the intensities at left and right sides are (3 $W \cdot cm^{-2}$ and 0 $W \cdot cm^{-2}$), (2.5 $W \cdot cm^{-2}$ and 0.5 $W \cdot cm^{-2}$), (2 $W \cdot cm^{-2}$ and 1 $W \cdot cm^{-2}$) and (1.5 $W \cdot cm^{-2}$ and 1.5 $W \cdot cm^{-2}$) for types I, II, III, and IV, respectively.

Figures 10a–d illustrate average power distribution vs. beef sample thickness in presence of ceramic supports for case 3 with all types of incidences (types I–IV) corresponding to $l_o = 0.1$ cm. For all types of microwave incidences, it is seen that the average power at R_1 mode is generally greater than that at R_2 mode. The maxima in average power within the sample may be dependent on various types of combinations in microwave sources and ceramic supports. It is seen that during R_1 mode, type I combinations correspond to larger average power: $q_{av,b} = 1.76$ $W \cdot cm^{-3}$ with no support, $q_{av,b} = 2.1$ $W \cdot cm^{-3}$ with Al_2O_3 support, $q_{av,b} = 1.14$ $W \cdot cm^{-3}$ with SiC support whereas for type IV combination of microwave incidence it is observed that $q_{av,b} = 1.17$ $W \cdot cm^{-3}$ with no support, $q_{av,b} = 1.29$ $W \cdot cm^{-3}$ with Al_2O_3 support, $q_{av,b} = 0.75$ $W \cdot cm^{-3}$ with SiC support as seen in Figure 10d. In general, Al_2O_3 support enhances the maxima in average power for types II–IV combinations whereas SiC support corresponds to smaller average power. For all types of incidences (I–IV) and specific oil thicknesses, the sample thickness corresponding to specific resonance mode is almost identical for no support and Al_2O_3 support cases, and the smaller thickness of sample is observed for SiC support. It is also interesting to note that, the sample thickness (L_s) corresponding to a resonance mode (R_1 or R_2) is the smaller in type I incidence.

Figures 11 illustrates the spatial distributions of amplitudes of electric fields, power and temperature for case 3 with no support during R_1 mode corresponding to type IV combinations as to demonstrate the effect of both sides incidence. Here,

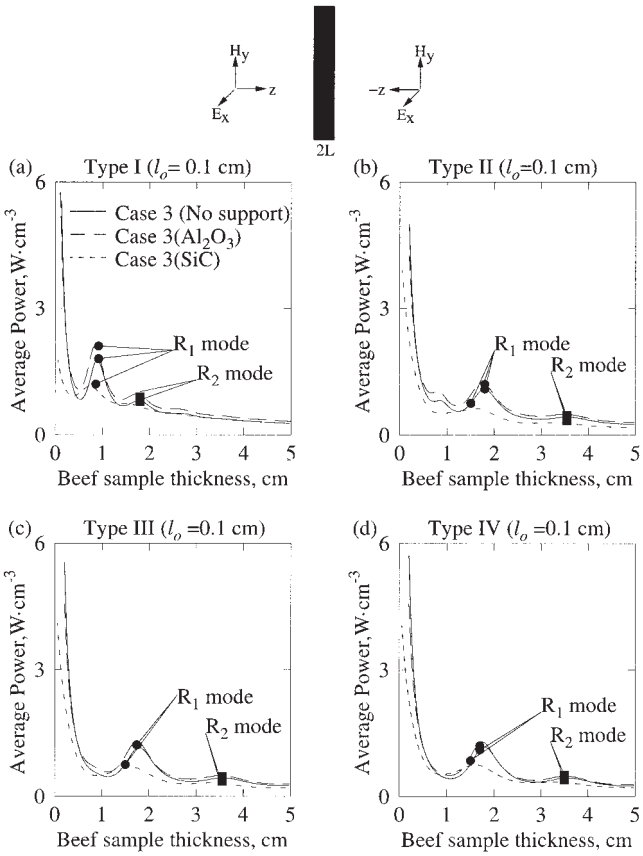

Figure 10. Average power in beef samples ($W \cdot cm^{-3}$) vs. sample thickness (cm) for case 3 without support and in presence of Alumina (Al_2O_3), and SiC supports for $l_o = 0.1$ cm with various types of microwaves incidence: (a) type I, (b) type II, (c) type III, (d) type IV.

The ceramic support thickness = 0.2 cm. $f = 2{,}450$ MHz, $I_L + I_R = 3$ $W \cdot cm^{-2}$. The filled circle denotes R_1 mode and the filled rectangle denotes R_2 mode of resonances. The average power for type I incidence with and without supports during R_1 and R_2 mode is larger than that with type II–IV incidences.

the distributions are shown for $l_o = 0.1$, 0.5, 1 and 2 cm. Similar to one-side incidence, it has been observed that the amplitude of transmitted wave is a decreasing function of distance, whereas the amplitude of reflected wave is an increasing function of slab depth within the beef sample. Similar to one side incidence, it is also observed that there is a significant jump in amplitudes of transmitted and reflected waves within the oil layer. Although total microwave intensity is 3 $W \cdot cm^{-2}$, the equidistribution of microwave sources at both the sides corresponds to smaller distribution of electric field and power. As a result, the average power within the beef sample is smaller than that with type I incidence as seen in Figures 3. Note that, the average powers in beef sample ($q_{av,b}$) are 1.17 $W \cdot cm^{-3}$, 1.20 $W \cdot cm^{-3}$, 1.25 $W \cdot cm^{-3}$ and 2.07 $W \cdot cm^{-3}$ corresponding to 0.1 cm, 0.5 cm, 1 cm and 2 cm, respectively.

The insets showing the difference in phase angle vs. distance within the slabs illustrate that three spatial resonances in microwave power corresponding to smaller thickness of oil ($l_o \leq 1$ cm) for type IV incidence, whereas two spatial resonances

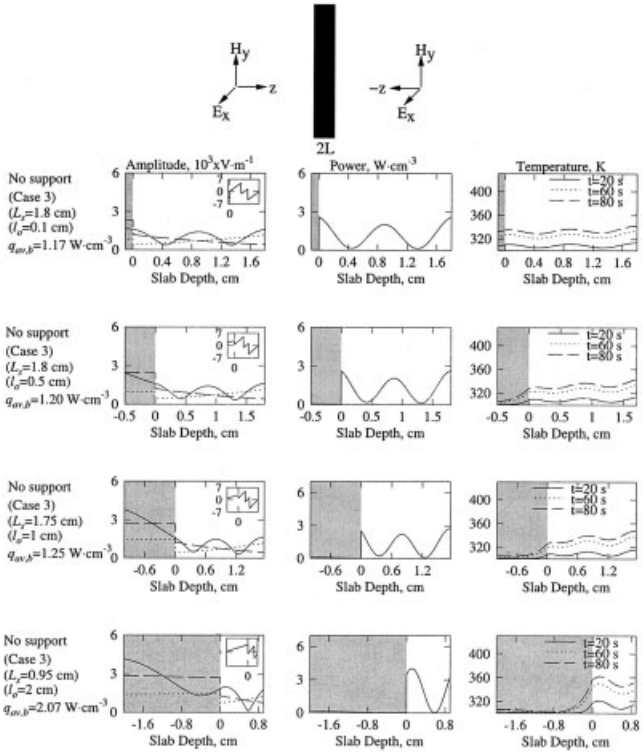

Figure 11. Amplitudes of electric field ($A_{x,l}$, $A^t_{x,l}$, $A^r_{x,l}$), power distributions and temperature profiles for case 3 in the absence of any support, where the samples exposed to microwaves from both the faces corresponding to type IV incidence during R_1 mode.

The shaded regime denotes the oil layer. Note that, various oil thicknesses are l_o = 0.1 cm, 0.5 cm, 1 cm, and 2 cm; — — —, transmitted wave; . . . . . , reflected wave; —, stationary wave. The inset shows phase difference ($\delta_{x,l}$) vs. z. f = 2,450 MHz, $I_L = I_R$ = 1.5 W · cm^{-2}. Greater heating rates are observed for larger oil thicknesses ($l_o \geq 1$ cm).

were observed for one side incidence case as seen in Figures 3 and 7. Similar to one side incidence, it has been observed that two spatial resonances in microwave power for greater oil thicknesses (l_o = 2 cm). Temperature distributions within the samples are illustrated by spatial temperature vs. sample thickness diagram as seen in Figures 11. During 80 s, the temperatures varies within 328–342 K, 327–344 K, 325–348 K, and 345–362 K for 0.1 cm, 0.5 cm, 1 cm and 2 cm thicknesses of oil, respectively. Similar to one side incidence, it is observed that greater thickness of oil may cause a runaway heating effect.

Figures 12 illustrates the amplitude, power and temperature distributions for case 3 during R_1 mode with Al_2O_3 support for various oil thicknesses with type IV microwaves incidence. The qualitative variations of amplitudes of the stationary and traveling waves are similar to that without support as seen in Figures 11. It is interesting to note that, the beef sample thicknesses (L_s) with Al_2O_3 support are generally smaller than that without the support whereas the average powers are generally larger with Al_2O_3 support. Note that, for $l_o \geq 1$ cm the degree of enhancement of average power absorption due to Al_2O_3 support is larger with type IV incidence which contrasts the one side incidence (type I) where the average power absorption is decreased due to Al_2O_3 support. It is interesting to observe that three spatial resonance in microwave power are observed with smaller thickness of oil ($l_o \leq 0.5$ cm) whereas two spatial resonances occur for $l_o \geq 1$ cm due to type IV incidence. Note that, the average powers in beef sample ($q_{av,b}$) are 1.29 W · cm^{-3}, 1.41 W · cm^{-3}, 1.65 W · cm^{-3} and 2.53 W · cm^{-3} corresponding to l_o = 0.1 cm, 0.5 cm, 1 cm and 2 cm, respectively. In contrast, for one side incidence (type I) the average power is greater for smaller oil thickness regimes ($l_o \leq 1$ cm) and smaller for larger oil thicknesses (l_o = 2 cm). Therefore, efficient microwave power absorption, and heating is highly dependent on various types of microwaves source combinations and supports. Temperature distributions within the samples are illustrated by spatial temperature vs. sample thickness. Here the temperatures are shown at 20 s, 60 s, and 80 s. During 80 s, the temperature varies within 326–346 K, 329–352 K, 333–352 K and 357–374 K for oil thicknesses 0.1 cm, 0.5 cm, 1 cm and 2 cm, respectively. It is observed that Al_2O_3 support may cause runaway heating specially for larger

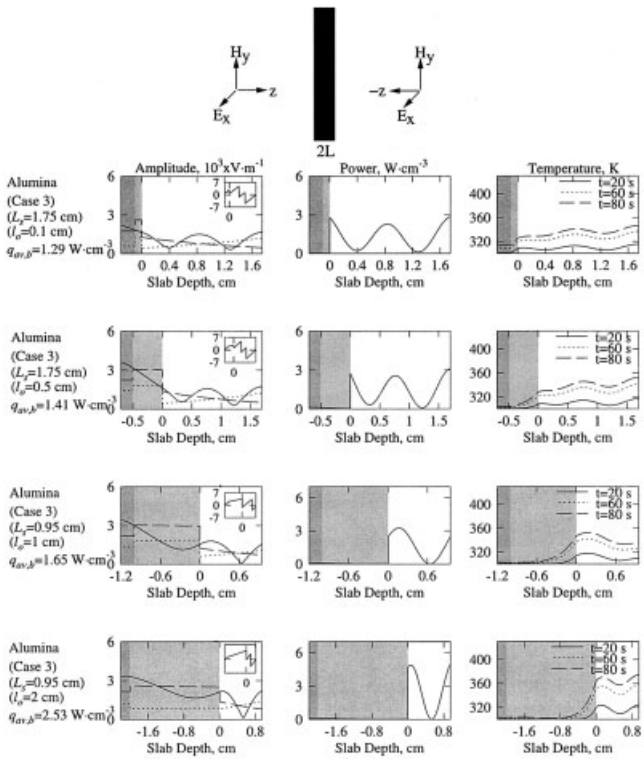

Figure 12. Amplitudes of electric field ($A_{x,l}$, $A^t_{x,l}$, $A^r_{x,l}$), power distributions and temperature profiles for case 3 with Alumina support where the samples are exposed to microwaves from both the faces corresponding to type IV incidence during R_1 mode.

The darker shaded regime denotes the support and the lighter shade denotes the oil layer. The thickness of support is 0.2 cm. Note that, various oil thicknesses are l_o = 0.1 cm, 0.5 cm, 1 cm, and 2 cm; — — —, transmitted wave; . . . . . , reflected wave; —, stationary wave. The inset shows phase difference ($\delta_{x,l}$) vs. z. f = 2,450 MHz, $I_L = I_R$ = 1.5 W · cm^{-2}. Greater heating rates are observed for larger oil thicknesses ($l_o \geq 1$ cm).

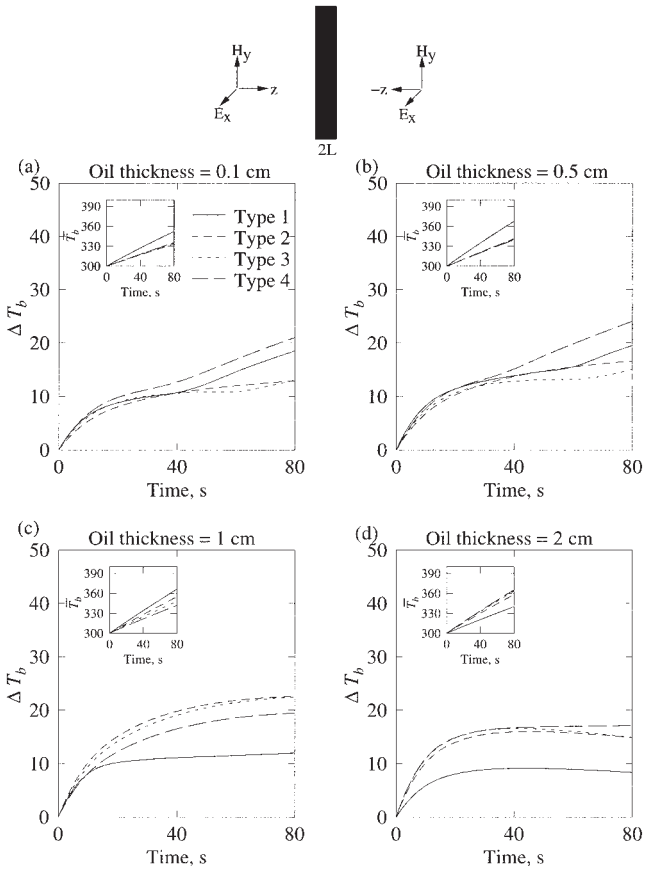

Figure 13. The temperature difference in beef samples, ΔT_b (K) vs. time (s) in presence of Alumina (Al_2O_3) support for samples incident with microwaves at both faces (case 3: type I–IV incidences) during R_1 mode for (a) l_o = 0.1 cm, (b) l_o = 0.5 cm, (c) l_o = 1 cm, and (d) l_o = 2 cm.

The insets denote the average temperature, $\overline{T_b}$ (K) vs. time (s). Type I incidence or one sided heating corresponds to less thermal runaway for larger thicknesses of oil ($l_o \geq 1$ cm).

oil thicknesses even with distributed microwave incidence (type IV).

Simulations were also carried out for case 3 during R_1 mode with SiC support (figures are not shown). It was observed that two spatial resonances in microwave power occur for $l_o \geq 0.5$ cm. During 80 s, the temperatures varies within 316–332 K, 321–328 K, 329–335 K and 335–347 K for 0.1 cm, 0.5 cm, 1 cm and 2 cm thickness of oil, respectively. The hot spot may occur at the side not attached to the support for $l_o \geq 2$ cm. SiC support with type IV incidence may reduce the heating rate within the beef sample; however, the heating process may avoid the runaway heating situation for less oil thicknesses.

Figures 13 illustrates the variation of temperature difference (ΔT_b) and average temperature ($\bar{T}_b$) within beef sample with time for cases 3 in presence of Al_2O_3 support for various oil thicknesses and types of incidences. The inset shows the average temperature ($\bar{T}_b$) vs. time plot. Figures 13a–b illustrate the distributions corresponding to smaller oil thicknesses ($l_o \leq 0.5$ cm). It is observed that the heating rates are greater with type I incidence and type II–IV incidences would correspond to identical heating rates. The temperature difference plot illustrate that types I and IV incidences would cause runaway heating during the later stages of heating whereas types II and III may cause temperature difference around 13–15 K during 80 s (Figures 13a–b). Figures 13c–d show the distributions for $l_o \geq 1$ cm. It is observed that one sided heating is a favorable heating process for beef samples with greater oil thicknesses as the runaway heating is lesser (ΔT_b = 8–10 K during 80 s).

Figures 14a–d illustrate the distributions of temperature difference and heating rate for beef samples for case 3 in presence of SiC support for various oil thicknesses and types of incidences. It is observed that the heating rate is larger with type I incidence irrespective of oil thicknesses. The temperature difference distribution illustrate that the runaway situation would occur with type I incidence at later stages. However, for $l_o \leq 0.5$ cm, the types II–IV incidences would cause less temperature difference. It is interesting to observe that type II incidence would cause lesser temperature difference for l_o = 2 cm. Therefore, the distributed heating sources may be efficient for heating composite beef-oil samples supported on SiC.

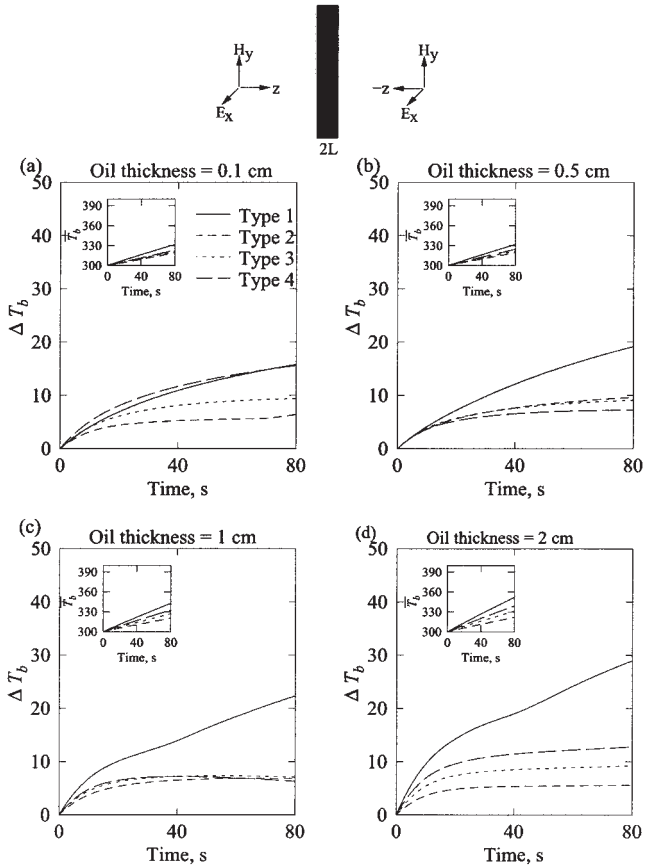

Figure 14. The temperature difference in beef samples, ΔT_b (K) vs. time (s) in presence of SiC support for samples incident with microwaves at both faces (case 3: type I–IV incidences) during R_1 mode for (a) l_o = 0.1 cm, (b) l_o = 0.5 cm, (c) l_o = 1 cm, and (d) l_o = 2 cm.

The insets denote the average temperature, $\overline{T_b}$ (K) vs. time (s). The distributed heating sources (type III–IV incidences) corresponds to less thermal runaway.

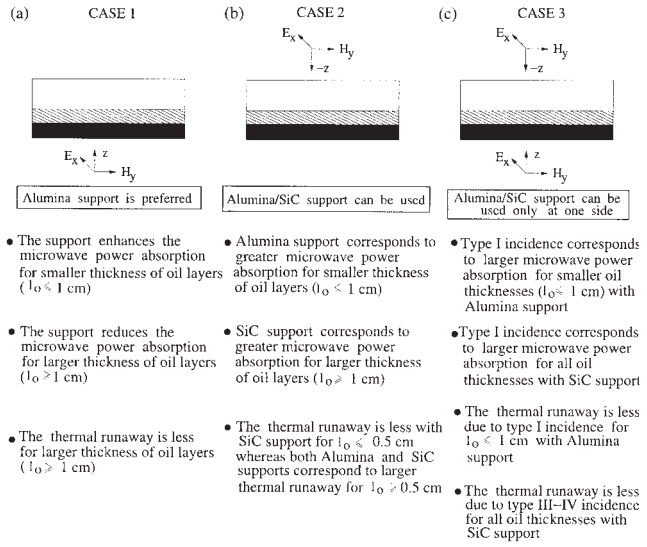

Figure 15. The heating characteristics for various sample-support assembly due to microwave radiations for (a) case 1, (b) case 2, and (c) case 3.

The darker shaded regime denotes the support, and the lighter shade represents oil layer.

Conclusions

We have carried out extensive analysis on microwave heating for beef-oil layered samples with and without ceramic supports due to microwaves incidence at one side and both the sides. For all these cases, the average power within beef samples vs. sample thickness distributions with various resonance modes (R_1 and R_2) are shown. Influence of various ceramic supports (Al_2O_3 and SiC) on average power distribution has been illustrated for various oil thicknesses. A detailed mathematical analysis has been carried out to study the role of individual traveling waves on spatial power and temperature for microwave heating in beef samples. Finally, the efficient microwave heating strategy has been illustrated with temperature difference (ΔT_b) and average temperature ($\bar{T}_b$) vs. time plot.

Figures 15a–c illustrate the efficient heating characteristics for cases 1, 2 and 3, respectively. Choice of support for efficient heating mechanism is highly sensitive with various heating mechanisms corresponding to cases 1–3. Alumina support is preferred for case 1 whereas Alumina or SiC support may be preferred for cases 2 and 3. For case 1 with Alumina support, larger heating rates within beef samples are observed for smaller thickness of oil layers, whereas the minima in thermal runaway is observed for larger thickness of oil layers. For case 2, Alumina support corresponds to higher heating rates for smaller thickness of oil layers, whereas SiC support corresponds to larger heating rates for larger thickness of oil layers. However, the thermal runaway is less with SiC support corresponding to smaller thickness of oil layer.

The efficient microwave heating of slabs are also analyzed for distributed microwave sources at both the sides (case 3). The spatial maxima in microwave power is a strong function of distributed microwave sources for various oil thicknesses. It is interesting to observe that Al_2O_3 support may cause runaway heating effects even with distributed microwave sources whereas SiC support may be preferred for distributed sources. It is interesting to observe that the distributed microwave sources at both the sides may reduce the runaway heating effects for specific cases. The efficient heating characteristics as seen in Figures 15a–c may be useful to provide a guideline for optimal microwave processing of composite materials.

Literature Cited

Ayappa, K. G., H. T. Davis, G. Crapiste, E. A. Davis, and J. Gordon, "Microwave Heating: An Evaluation of Power Formulations," *Chem. Eng. Sci.,* **46**, 1005 (1991).

Ayappa, K. G., H. T. Davis, E. A. Davis, and J. Gordon, "Two-Dimensional Finite Element Analysis of Microwave Heating," *AIChE J.,* **38**, 1577 (1992).

Ayappa, K. G., H. T. Davis, S. A. Barringer, and E. A. Davis, "Resonant Microwave Power Absorption in Slabs and Cylinders," *AIChE J.,* **43**, 615 (1997).

Ayappa, K. G., "Resonant Microwave Power Absorption in Slabs," *J. Microwave Power and E. M. Energy,* **34**, 33 (1999).

Basak, T., and K. G. Ayappa, "Analysis of Microwave Thawing of Slabs With Effective Heat Capacity Method," *AIChE J.,* **43**, 1662, 7 (1997).

Basak, T., and K. G. Ayappa, "Influence of Internal Convection During Microwave Thawing of Cylinders," *AIChE J.,* **47**, 835 (2001).

Basak, T., and K. G. Ayappa, "Role of Length Scales on Microwave Thawing Dynamics in 2D Cylinders," *Int. J. Heat and Mass Transfer,* **45**, 4543 (2002).

Basak, T., "Analysis of Resonances During Microwave Thawing of Slabs," *Int. J. Heat and Mass Transfer,* **46**, 4279 (2003).

Basak, T., "Role of Resonances on Microwave Heating of Oil-Water Emulsions," *AIChE J.,* **50**, 2659 (2004a).

Basak, T., "Analysis of Microwave Propagation for Multilayered Material Processing: Lambert's Law versus Exact Solution," *Industrial & Eng. Chem. Research,* **43**, 7671 (2004b).

Basak, T., and A. S. Priya, "Role of Ceramic Supports on Microwave Heating of Materials," *J. Appl. Phys.,* **97**, 083537 (2005).

Chamchong, M., and A. K. Datta, "Thawing of Foods in a Microwave Oven: I. Effect of Power Levels and Power Cycling," *J. Microwave Power and EM Energy,* **34**, 9 (1999a).

Chamchong, M., and A. K. Datta, "Thawing of Foods in a Microwave Oven: II. Effect of Load Geometry and Dielectric Properties," *J. Microwave Power and EM Energy,* **34**, 22 (1999b).

Chatterjee, A., T. Basak, and K. G. Ayappa, "Analysis of Microwave Sintering of Ceramics," *AIChE J.,* **44**, 2302 (1998).

Lee, M. Z. C., and T. R. Marchant, "Microwave Thawing of Cylinders," *Applied Math. Modelling,* **28**, 711 (2004).

Massoudi, H., C. H. Durney, P. W. Barber, and M. F. Iskander, "Electromagnetic Absorption in Multilayered Cylinder Models of Man," *IEEE Trans. Microwave Theory and Techniques,* **27**, 825 (1979).

Ohlsson, T., and P. O. Risman, "Temperature Distribution of Microwave Heating-Spheres and Cylinders," *J. Microwave Power,* **13**, 303 (1978).

Rattanadecho, P., "Theoretical and Experimental Investigation of Microwave Thawing of Frozen Layer using a Microwave Oven (Effects of Layered Configurations and Layer Thickness)," *Int. J. Heat and Mass Transfer,* **47**, 937 (2004).

Shin, G. I., Y. K. Yeo, B. Y. Jo, H. Y. Kim, and V. V. Levdansky, "Analysis on Effects of Microwave Heating in Porous Catalysts," *J. Chem. Eng. Japan,* **12**, 1567 (2001).

Weil, C. M., "Absorption Characteristics of Multilayered Sphere Models Exposed to UHF/Microwave Radiation," *IEEE Trans. Biomed. Eng.,* **BME-22**, 468 (1975).

Xu, Y. Y., Z. Min, A. S. Mujumdar, L. Q. Zhou, and J. C. Sun, "Studies on Hot Air and Microwave Vacuum Drying of Wild Cabbage," *Drying Technology,* **22**, 2201 (2004).

Manuscript received May 23, 2005, and revision received Dec. 7, 2005.